Artificial Neural Network Prediction of Aerosol Deposition in Human Lungs

Javed Nazir,[1] David J. Barlow,[1,4] M. Jayne Lawrence,[1] Christopher J. Richardson,[2] and Ian Shrubb[3]

Received April 4, 2002; accepted April 23, 2002

Purpose. To develop a rapid and reliable method for predicting the pattern of aerosol particle deposition within the human lungs, using artificial neural networks (ANNs).

Methods. Experimental data from the literature were used to train multi-layer perceptron (MLP) networks to allow for prediction of regional and total aerosol particle deposition patterns in human lungs. These data covered particle sizes in the range 0.05–15 μm and three different breathing patterns (ranging from "quiet" breathing to breathing "under physical work conditions"). Three different MLPs were trained, to provide separate predictions of aerosol particle deposition in the laryngeal, bronchial, and alveolar regions. The total deposition fraction for a given set of breathing conditions was computed simply as the sum of the outputs produced from the corresponding regional deposition MLPs.

Results. The ANNs developed are shown to give highly accurate predictions for both regional and total aerosol deposition patterns for all particle sizes and breathing conditions (with errors typically less than 0.04%).

Conclusions. We conclude that the current set of ANNs can be used to give good predictions of particle deposition from polydisperse pharmaceutical aerosols generated from breath-actuated dry powder inhalers, nebulizers, and metered dose inhalers with spacers.

KEY WORDS: artificial neural networks; aerosol deposition; human lungs.

INTRODUCTION

For many years now, formulation scientists have been concerned with the problem of how best to administer medical aerosols to maximize delivery of therapeutic agents to infected regions of lung diseased patients (1). A variety of different medical aerosols devices have been devised, including nebulizers and dry-powder and metered dose inhalers (2–4). However, the efficacy of these devices in pulmonary drug delivery is still fairly unpredictable (5). It is generally the case that a significant amount of administered drug does not reach the target sites, but is instead deposited within the throat and upper respiratory tract due to inertial impaction, sedimentation, and diffusion mechanisms.

For this reason (together with the interest in inhaled pollutants), aerosol deposition in humans has been subjected to many years of experimental and theoretical investigation. While numerous reviews on *in vivo* experimental studies have been reported (6), the most extensive data published to date remain those given by Heyder *et al.* (7), who carried out a systematic series of laboratory tests involving human volunteers, measuring the regional and total deposition fractions of inhaled particles of defined sizes under well-defined breathing conditions.

Over the years, both stochastic (Monte Carlo) and deterministic (computational fluid dynamics) models have been developed in efforts to predict the patterns of aerosol particle deposition in human lungs, and the human subject data of Heyder *et al.* (7) have frequently been employed in validating these models (8–9). In all such modeling, however, the calculations involved are highly complex and require significant computing resource. Many also involve simplifying approximations such as a symmetric lung morphology (10) and so have limited utility in making predictions for real systems.

In this study, which builds on our earlier work (11), we have sought to develop a more reliable and more rapid method for predicting the pattern of aerosol particle deposition within the human lungs, using artificial neural networks (ANNs).

ANNs are now widely used in problem-solving, in many diverse fields in science and engineering, among them pattern recognition and classification, signal and image processing, robot control, geography (12), financial forecasting (13), and medical diagnosis (14). ANNs are also being successfully applied to solve numerous problems in the pharmaceutical sciences arena, including molecular graphics (15), quantitative structure-activity relationships (16), pharmaceutical formulation (17), pharmacokinetics (18), and drug dissolution profiles (19).

In general, ANNs try to replicate the way the human brain processes information. Instead of being programmed by a user in a traditional sense, ANNs are constructed so that they can be "trained" to perform a particular task, most often being required to relate the input and output variables of the problem (20). Basically, the concept is very simple. An input pattern is presented to the ANN and the corresponding network output is computed. This output is then compared to the desired output (or target) for that pattern and an error is found. ANN training then proceeds in such a way as to minimize the error between the calculated output and the desired output.

In this research, experimental data from the human subject studies of Heyder *et al.* (7) were used to train neural networks to allow for prediction of regional and total aerosol deposition patterns in human lungs. The deposition data presented in their paper represent mean values for lung deposition fractions of monodisperse unit density aerosols for three healthy subjects during nose and mouth breathing. In each laboratory test, the subjects were asked to inspire at a prescribed constant flow rate up to a given tidal volume, then exhaled at a similar flow rate, with no irregular pauses between inspiratory and the expiratory periods of a breath. In our work, as a preliminary step we have been concerned with using only data from the oral breathing experiments for which regional deposition fractions were measured under three different breathing patterns and with particle sizes in the range 0.05–15 μm.

[1] Department of Pharmacy, King's College London, The Franklin Wilkins Building, 150 Stamford Street, London SE1 9NN, United Kingdom.

[2] The Institute of Cancer Research, 123 Old Brompton Road, London SW7 3RP, United Kingdom.

[3] AstraZeneca R&D Charnwood, Pharmaceutical & Analytical R&D, Bakewell Road, Loughborough, Leicestershire LE11 5RH, United Kingdom.

[4] To whom correspondence should be addressed. (e-mail: dave.barlow@kcl.ac.uk)

0724-8741/02/0800-1130/0 © 2002 Plenum Publishing Corporation

Table I. Mean Square Error Achieved in Prediction of Laryngeal Deposition of Aerosols, Given Different ANN Configurations

ANN configurations[a]	Mean square error achieved	
	Training set[b]	Test set[b]
3–2–1	0.0000872	0.000293
3–3–1	0.0000792	0.000270
3–4–1	0.0000666	0.000306
3–5–1[c]	0.0000505	0.000197
3–6–1	0.0000612	0.000281
3–7–1	0.0000645	0.000280
3–8–1	0.0000579	0.000290

[a] ANN configurations are presented as m–n–l, where m, n, and l are respectively, the number of neurons in the input, hidden, and output layers of the networks.
[b] Mean square errors achieved at point of minimum cross-validation error.
[c] ANN configuration chosen as optimal.

MATERIALS AND METHODS

The implementation and training of the neural networks were carried out using a new Windows© based version of the pulmonary drug delivery learning engine, PUDDLE (11). All the ANNs developed use MLP network topology (20). In general, MLP networks consist of one input layer, one or more hidden layers and one output layer, with each layer made up of a number of artificial neurons called nodes. The nodes in adjacent layers are fully interconnected and each connection's "strength" is determined by its connection weight.

At the start of training, the connection weights and biases are assigned random values typically in the range 0 to 1. During training, changes in the connection weights and biases are achieved by back propagation of error. In other words, the calculated output of the network (O) is compared with the desired output or target (T) to determine the associated error for that input pattern. Using this error, a factor is computed that is used to distribute the error at the output back to all the nodes in the previous layers.

In this study, back-propagation of error is carried out using batch training, that is, the necessary changes to connection weights and biases are calculated and updated after all the input-target pairs in the training set (N') have been tested. Training proceeds until the number of iterations exceeds a specified maximum, or until the mean square error on the training set reaches a defined minimum. The mean square error, ε is calculated as:

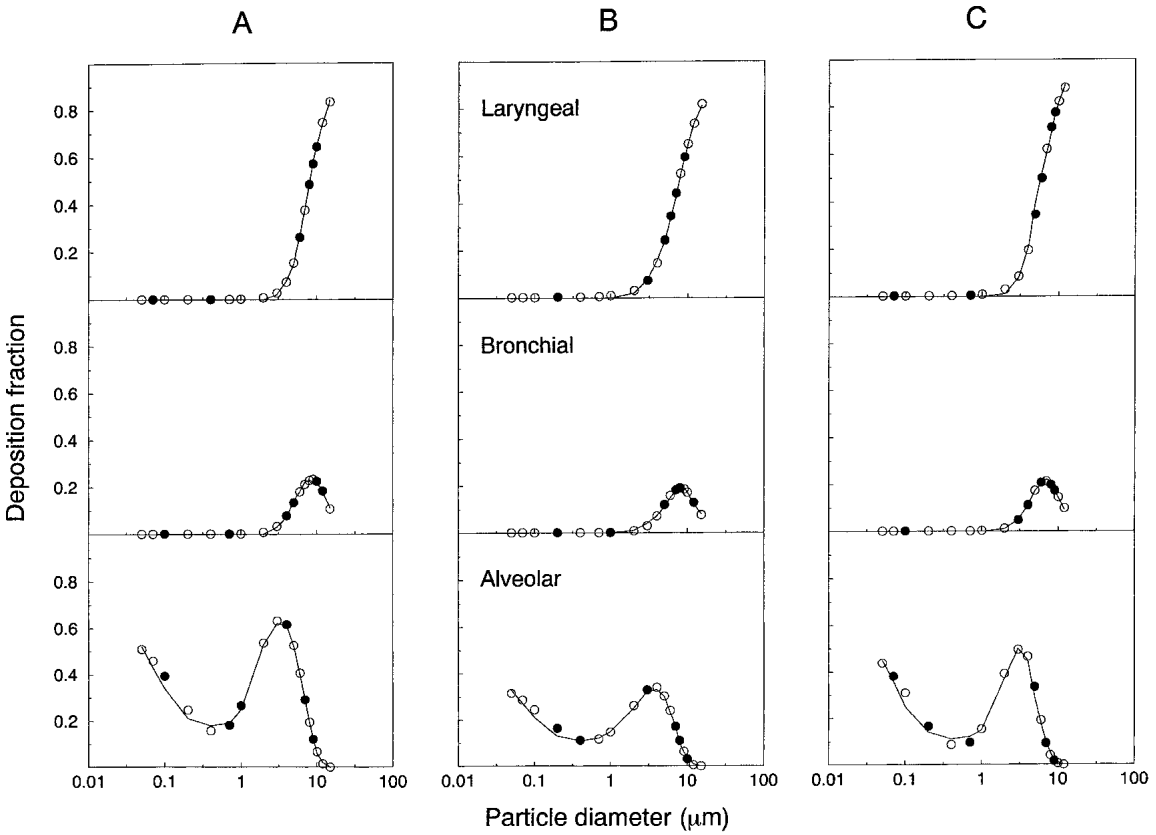

Fig. 1. Comparison of predicted and measured deposition patterns of unit density spheres within the human respiratory tract during oral breathing. Graphs in column A are for the breathing conditions: 1000 mL tidal volume, 8 s breathing cycle period, and 250 mL/s inspiratory flow rate. Graphs in column B are for the breathing conditions: 500 mL tidal volume, 4 s breathing cycle period, and 250 mL/s inspiratory flow rate. Graphs in column C are for the breathing conditions: 1500 mL tidal volume, 4 s breathing cycle period, and 750 mL/s inspiratory flow rate. In each column the upper, center and lower panels show data for laryngeal, bronchial and alveolar deposition, respectively. The solid lines represent the experimental data from Heyder et al. (1986). The open circles show the data used in the MLP training and the filled circles, the MLP predictions for test/cross-validation data.

$$\varepsilon = \frac{\sum_{k=1}^{k=N'} (T_k - O_k)^2}{N'} \quad (1)$$

where k = 1 to N′ are the input-output patterns, N′ is the number of desired targets, T_k is the k^{th} element of the target in the training set, and O_k is the k^{th} element of the computed network output.

[For further details of the principles and basic methodology involved in the development of MLPs, refer to references (11) and (20).]

When training MLPs, it is important to ensure that the optimized weights reach the global minimum and do not become trapped in one of the many local minima that make up the error landscape. To avoid this situation, the time-invariant noise algorithm (TINA) of Burton and Mpitsos was implemented (21). TINA serves both to enhance the rate of learning and improve the final error achieved by the MLP networks. This algorithm is based on the principle of simulated annealing (that is, injection of random noise during the training process), but is time independent. The level of injected noise is dependent on the error associated with the network output rather than the number of iterations that have passed. At the outset of training, the level of injected noise is high (due to a training error), but as training proceeds, the training error gradually decreases and so does the level of injected noise. As a result, the network converges towards the global minimum. TINA is implemented simply by an additional term in the adjustment of connection weights and biases calculated as:

$$\Delta W = nr(T_k - O_k)^2 \quad (2)$$

where ΔW is the additional adjustment to connection weights and biases, n is a constant determining the level of noise at the start of training, and r is a number chosen randomly from a uniform linear distribution in the range −1 to +1.

It should be emphasized here, however, that the attainment of a global minimum error does not necessarily imply that the trained network will be able to generalize from the training patterns provided, that is, it will not guarantee accurate predictions when the network is presented with previous unseen data. The network could simply have memorized and overfitted the training data. To avoid this problem, we have implemented the technique of "split-sample" cross-validation during training of the MLP networks. In short, the data used are divided into three sets; a training set, a cross validation set and a test set. The network weights and biases are updated after all the input-output patterns in the training set have been presented to the network, and the error associated with the cross validation data set is monitored. Typically, the cross-validation error will initially decrease as the network model achieves a better fit to the data, but later, when the network begins to overfit, the cross-validation error starts to rise. The connection weights and biases for the best-trained network are taken to be those existing when the minimum in cross-validation error is achieved.

The data employed in training the networks were taken from Heyder *et al.* (7). Particle diameter, breathing cycle period, and mean inspiratory flow rate were provided to the network as input (each normalized to lie within the range 0–1), and the target output consisted of the aerosol particle regional deposition fractions. The network inputs were se-

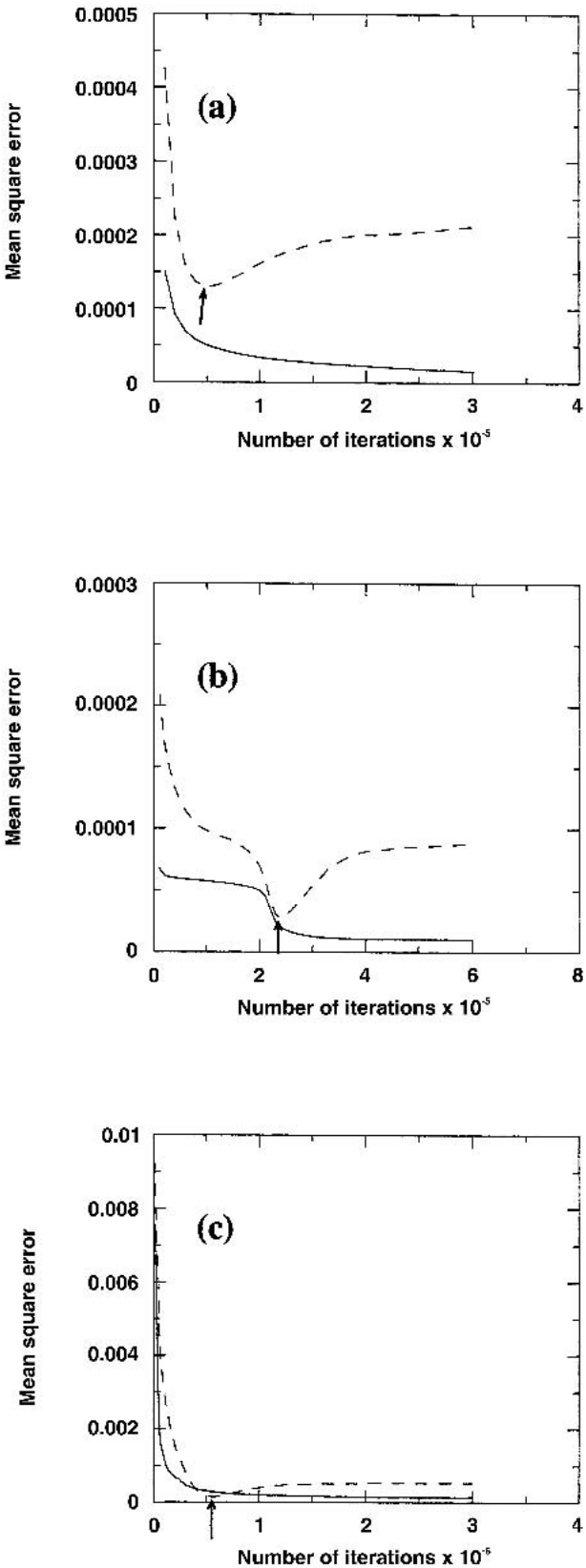

Fig. 2. Mean square error as a function of number of iterations for the 3 MLP networks used. (a) Network I (laryngeal deposition). (b) Network II (bronchial deposition). (c) Network III (alveolar deposition). The solid and dashed lines are, respectively, the training error and cross validation error. Arrows indicate positions of minimum cross validation error.

Table II. Comparison of ANN Output and Associated Errors with Results Obtained Using Stochastic and Deterministic Models

Condition 1[b]	Total deposition fraction[a]				
Particle size (μm)	Experimental data	ANN (% error)	Stochastic-1 (% error)	Stochastic-2 (% error)	Deterministic (% error)
0.050	0.52	0.51 (–1.7)	0.55 (5.8)	0.55 (5.8)	0.64 (23.1)
0.100	0.34	0.39 (16.0)	0.42 (23.5)	0.42 (23.5)	0.41 (20.6)
0.200	0.21	0.25 (18.3)	0.22 (4.8)	0.22 (4.8)	0.25 (19.0)
0.400	0.18	0.16 (–11.6)	0.14 (–22.2)	0.14 (–22.2)	0.16 (–11.1)
0.700	0.18	0.18 (1.7)	0.23 (27.8)	0.23 (27.8)	0.16 (–11.1)
1.000	0.25	0.27 (7.8)	0.36 (44.0)	0.36 (44.0)	0.20 (–20.0)
2.000	0.53	0.55 (4.5)	0.52 (–1.9)	0.50 (–5.7)	0.48 (–9.4)
5.000	0.81	0.81 (0.3)	0.75 (–7.4)	0.73 (–9.9)	0.83 (2.5)
10.000	0.93	0.94 (0.7)	0.88 (–5.4)	0.92 (–1.1)	0.92 (–1.1)
Condition 2[c]					
0.050	0.33	0.32 (–3.3)	0.34 (3.0)	0.34 (3.0)	0.43 (30.3)
0.100	0.21	0.25 (18.0)	0.19 (–9.5)	0.19 (–9.5)	0.25 (19.0)
0.200	0.13	0.17 (28.6)	0.12 (–7.7)	0.12 (–7.7)	0.14 (7.7)
0.400	0.11	0.12 (6.7)	0.08 (–27.3)	0.08 (–27.3)	0.09 (–18.2)
0.700	0.12	0.12 (3.5)	0.09 (–25.0)	0.09 (–25.0)	0.08 (–33.3)
1.000	0.15	0.16 (5.5)	0.13 (–13.3)	0.13 (–13.3)	0.10 (–33.3)
2.000	0.28	0.30 (6.3)	0.28 (0.0)	0.27 (–3.6)	0.24 (–14.3)
5.000	0.65	0.66 (2.1)	0.50 (–23.1)	0.49 (–24.6)	0.66 (1.5)
10.000	0.86	0.85 (–0.9)	0.73 (–15.1)	0.81 (–5.8)	0.85 (–1.2)
Condition 3[d]					
0.050	0.45	0.44 (–2.0)	0.54 (20.0)	0.54 (20.0)	0.52 (15.6)
0.100	0.25	0.31 (24.8)	0.31 (24.0)	0.31 (24.0)	0.30 (20.0)
0.200	0.14	0.17 (20.0)	0.14 (0.0)	0.14 (0.0)	0.17 (21.4)
0.400	0.11	0.09 (–17.3)	0.12 (9.1)	0.12 (9.1)	0.11 (0.0)
0.700	0.12	0.10 (–14.9)	0.13 (8.3)	0.13 (8.3)	0.11 (–8.3)
1.000	0.15	0.16 (8.4)	0.22 (46.7)	0.23 (53.3)	0.13 (–13.3)
2.000	0.39	0.43 (11.0)	0.55 (41.0)	0.37 (–5.1)	0.32 (–17.9)
5.000	0.86	0.85 (–0.8)	0.77 (–10.5)	0.82 (–4.7)	0.82 (–4.7)
10.000	0.97	0.97 (0.0)	0.92 (–5.2)	0.98 (1.0)	0.96 (–1.0)

[a] Experimental data from Heyder et al. (7). Stochastic-1 and stochastic-2 results taken from Hofmann et al. (8) (calculated using equations from refs. 22 and 6, respectively). The deterministic results are from Martonen et al. (23).
[b] TV = 1000 mL, T = 4 s, and Q = 250 mL/s.
[c] TV = 500 mL, T = 4 s, and Q = 250 mL/s.
[d] TV = 1500 mL, T = 4 s, and Q = 750 mL/s.

lected through a simple consideration of the known factors influencing the site and extent of aerosol deposition, *viz*., the sizes of the particles, their residence time within the airways, and the velocity of the air in which they are borne along within the airways (6). An MLP network consisting of three input nodes, four hidden nodes, and one output node was found adequate for predicting bronchial deposition, whereas both laryngeal and alveolar deposition data necessitated the use of a 3–5–1 configuration. These network configurations were obtained after extensive experimentation with networks of varying complexities (that is, varying number of hidden neuron layers and varying number of hidden neurons per layer), with the network momentum (α), learning rate (β), and noise level (n) in each case adjusted manually to give optimum training performance. The final set of network configurations was chosen based on consideration of the mean square errors achieved for the training, test, and cross-validation data sets. Table I, for example, shows the case for laryngeal deposition. Here, the mean square errors achieved in ANN predictions are given as a function of the number of neurons in a single hidden layer (varied from 2 to 8). It will be noted that for the final configuration chosen (3–5–1), when the minimum in cross-validation error is achieved the mean square errors for the training and test data sets are lower than those achieved with any other network configuration.

For all three of the networks, 70% of the input data were used for training, 10% for cross-validation and the remaining 20% for the test set. The three networks were trained to provide predictions for laryngeal, bronchial, and alveolar deposition fractions, respectively. The total deposition fraction for a given set of breathing conditions was computed simply as the sum of the outputs produced from the corresponding regional deposition ANNs.

RESULTS AND DISCUSSION

All three aerosol particle deposition networks were trained on a 700MHz PC equipped with 128Mb RAM; the training in each case was completed in under 3 m. Figure 2 shows the mean square error achieved as a function of training iteration. It will be noted (as discussed before) that although the errors associated with the networks' predictions

for the training set data decreased more or less continuously, the corresponding errors for the predictions made for the cross-validation data initially decreased and then increased. Because the increasing errors in the cross-validation data predictions are associated with over-training of the neural networks, the weights and biases taken, as those of the best-trained networks were those existing at the point when minimum cross-validation errors were achieved. For laryngeal, bronchial, and alveolar networks these minima were reached after 50,000, 240,000, and 560,000 iterations, respectively (at the points indicated by arrows in Fig. 2).

In Figure 1 we compare the predicted patterns of aerosol particle deposition against those determined experimentally by Heyder *et al.* (7). Column A shows the deposition patterns resulting from "quiet breathing", with a slow inspiration over a relatively long time (tidal volume TV = 1000 mL, breathing cycle period T = 8 s, mean inspiratory flow rate Q = 250 mL/s). Column C shows the corresponding patterns arising for breathing under "physical work conditions" (TV = 1500 mL, T = 4 s, Q = 750 mL/s), and those in Column B are for "intermediate" conditions (TV = 500 mL, T = 4 s, Q = 250 mL/s).

In all cases, and for all sizes of particles, it will be seen that the MLP networks are able to follow closely and accurately the changes in regional lung deposition fractions. The mean errors associated with the networks' predictions (calculated only over the "unseen" data) are 0.012%, 0.009%, and 0.035%, for the laryngeal, bronchial, and alveolar particle deposition, respectively. The predictions made are significantly better than those achieved using either stochastic or deterministic models (see Table II) – even for the case of small particle deposition under "physical work conditions" (where the ANN predictions for total deposition are at their worst, on average, ~11%) (6,8,22–24).

Accepting then that the ANNs have been trained successfully we take the further step of making predictions of the regional and total deposition fractions of inhaled particles following changes in breathing conditions. We first consider the effects of changes in respiratory time and tidal volume when inspiratory flow rate remains the same, and then consider the effects of changes in inspiratory flow rate when breathing cycle period is kept constant. The results obtained in these predictions are depicted in Figs. 3, 4, and 5.

From Fig. 3, we see that at a given inspiratory flow rate, the total lung deposition fraction increases with an increase in respiratory time for all particles with sizes in the range 1–5 μm, a result which accords well with the experimental findings reported by Kim (25). These changes primarily reflect the increase in alveolar deposition (Fig. 3c) and are accounted for by the fact that the residence time of the aerosols in the lung is longer and so the particles have a greater likelihood of being deposited through gravitational sedimentation. Moreover, since the flow rate here is kept constant, the increase in breathing cycle period is tantamount to an increase in tidal volume, with the consequence that this leads to the inhaled particles penetrating more deeply into the lungs, and this in turn gives greater opportunity for their deposition.

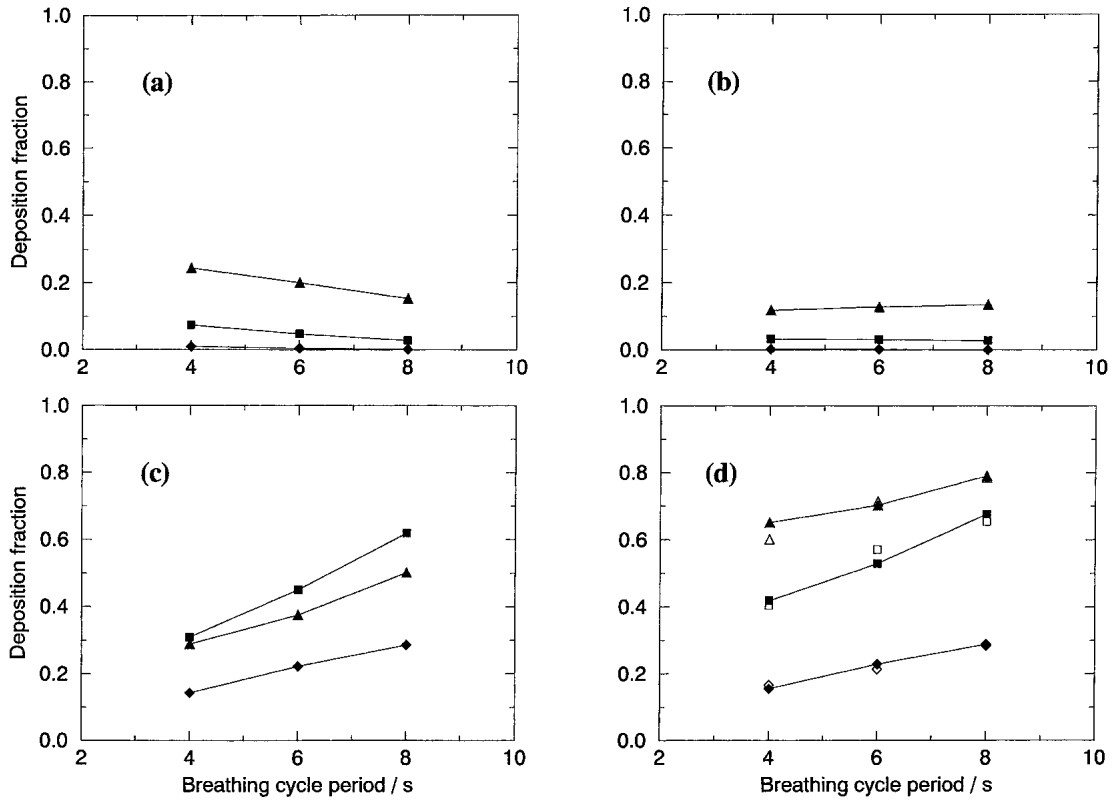

Fig. 3. Regional and total lung deposition fractions for three sizes of inhaled particles (*diamonds* 1 μm; *squares* 3 μm; and *triangles* 5 μm) as a function of breathing cycle period, at a fixed value of inspiratory flow (Q = 250 mL/s). (a) Laryngeal deposition fraction. (b) Bronchial deposition fraction. (c) Alveolar deposition fraction. (d) Total lung deposition fraction. In (a)–(d) the filled symbols show the MLP predictions and in (d) the open symbols show the experimental data taken from (25). Lines shown are intended only as a guide to the eye.

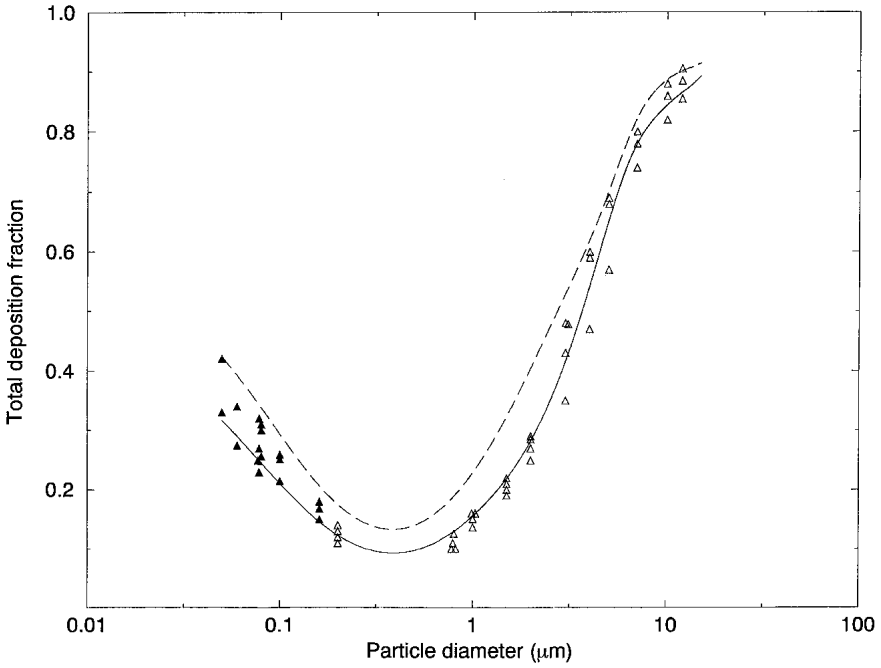

Fig. 4. Total lung deposition fraction as a function of particle size for two different breathing conditions, where the tidal volume, TV = 500 mL (solid line) or 750 mL (dashed line), in both cases with inspiratory flow rate, Q = 250 mL/s. The lines show the MLP predictions and the points plotted are the experimental data (for the case where TV = 500 mL) taken from ref. 6, originally presented by Heyder et al. (7) and Schiller et al. (24).

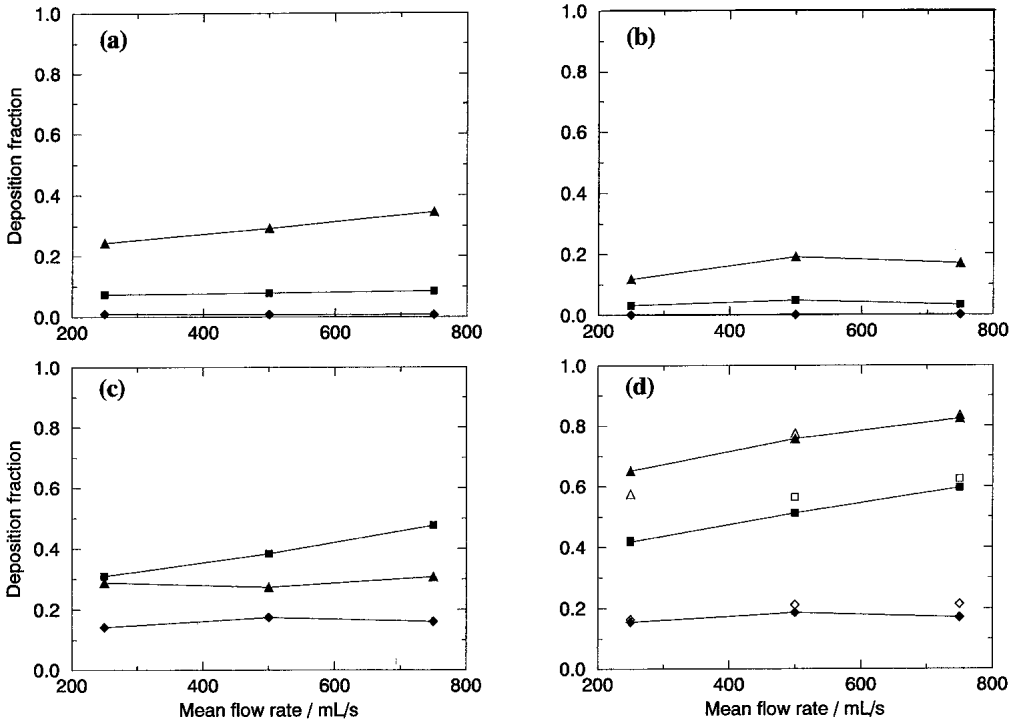

Fig. 5. Regional and total lung deposition fractions for three sizes of inhaled particles (*diamonds* 1 μm; *squares* 3 μm; and *triangles* 5 μm) as a function of inspiratory flow rate, at a fixed value of respiratory time (T = 4 s). (a) Laryngeal deposition fraction. (b) Bronchial deposition fraction. (c) Alveolar deposition fraction. (d) Total lung deposition fraction. In (a)– (d) the filled symbols show the MLP predictions and in (d) the open symbols show the experimental data taken from (25). Lines shown are intended only as a guide to the eye.

In Fig. 4 we show the total lung deposition fraction versus aerosol particle diameter as TV increases with a given inspiratory flow rate (250 mL/s). The U-shaped curve for the total lung deposition fraction is seen to shift upwards as TV increases (from 500 mL to 750 mL), but with the deposition minimum always found for particles of ≈ 0.5 μm. Here too, the network predictions for a given set of breathing conditions compare favorably with the available experimental data (6,7,24), and the shift in the curve caused on changing the breathing conditions is just as reported by Kim (25). The fact that the deposition fraction for 0.5 μm particles remains as a minimum regardless of TV is explained by the fact that none of the 3 mechanisms (inertial impaction, gravitational sedimentation, and diffusion) acts strongly on these particles. Larger particles (>0.5 μm) are greatly influenced by inertial impaction and gravitational sedimentation, whilst smaller particles (<0.5 μm) are deposited effectively by diffusion.

When the inspiratory flow rate is varied at a constant respiratory time the predicted effects on regional and total deposition fractions are as illustrated in Fig. 5. Once again the network predictions are within 10% of the recorded experimental data (25). The total lung deposition fraction (Fig. 5d) increases with flow rate for particles of 3 μm in size and above, whereas for particles of 1μm in diameter, the deposition fraction is independent of inspiratory flow rate. This can be explained by the fact that the deposition of small particles in the lungs is mainly governed by gravitational sedimentation and diffusion and these mechanisms are independent of inspiration flow.

CONCLUSIONS

The work presented here has demonstrated that ANNs can be successfully employed to predict regional and total aerosol particle deposition patterns in human lungs, given that there is sufficient data to train the networks. It is important to note that the neural networks designed in this study were trained on data for only three breathing conditions for which regional and total deposition fractions are available (7). The predictions for regional and total aerosol particle deposition fractions are thus reliable only within the following ranges: particle diameters 0.05 to 15 μm; breathing cycle periods 4 to 8 s; inspiratory flow rates 250 to 750 mL/s; tidal volumes 500 to 1500 mL.

In terms of the development of such tools to aid in the evaluation and design of pulmonary drug delivery systems, however, these limitations are not considered serious. The limits on breathing conditions span the whole of the relevant range from "quiet breathing" through to "breathing under physical work", and the limits on particle sizes more than cover the particle size ranges which are typical in polydisperse medical aerosols, where the mass median aerodynamic diameters are quoted to be 1–3 μm (25).

It must be noted, however, that the ANNs reported here are appropriate only for passive breathing, and so are applicable to pharmaceutical aerosols generated by certain devices only (i.e., solid powders from breath-actuated DPIs, nebulized droplets from nebulizers, and pressurized aerosols from MDIs with spacers).

ACKNOWLEDGMENTS

J. N. gratefully acknowledges financial support from Astra Zeneca.

REFERENCES

1. J. S. Patton. Mechanisms of macromolecule absorption by the lung. *Adv. Drug Deliv. Rev.* **19**:3–36 (1996).
2. I. Ashurst, A. Malton, D. Prime, and B. Sumby. Latest advances in the development of dry powder inhalers. *Pharm. Sci. Technol. To.* **3**:246–256 (2000).
3. K. J. McDonald and G. P. Martin. Transitions to cfc-free metered dose inhalers-into the millennium. *Int. J. Pharm.* **201**:89–107 (2000).
4. R. N. Lawrence. Intelligent inhalers for systemic administration? *Drug Discov. Today* **6**:445–446 (2001).
5. M. L. Everard. Aerosol therapy past, present, and future: a clinician's perspective. *Respiratory Care* **45**:769–776 (2000).
6. W. Stahlhofen, G. Rudolf, and A. C. James. Intercomparison of experimental regional aerosol deposition data. *J. Aerosol Med.* **2**:285–308 (1989).
7. J. Heyder, J. Gebhart, G. Rudolf, C. F. Schiller, and W. Stahlhofen. Deposition of particles in the human respiratory tract in the size range 0.005-15μm, J. *Aerosol Sci.* **17**:811–825 (1986).
8. W. Hofmann and L. Koblinger. Monte carlo modeling of aerosol deposition in human lungs. Part III: Comparison with experimental data. *J. Aerosol Sci.* **23**:51–63 (1992).
9. T. B. Martonen, C. J. Musante, R. A. Segal, J. D. Schroeter, D. Hwang, M. A. Dolovich, R. Burton, R. M. Spencer, and J. S. Fleming. Lung models: Strengths and limitations. *Respiratory Care* **45**:712–736 (2000).
10. E. Weibel. *Morphometry of the human lung*. Springer-Verlag, Berlin, 1963.
11. C. J. Richardson and D. J. Barlow. Neural network computer simulation of medical aerosols. *J. Pharm. Pharmacol.* **48**:581–591 (1996).
12. G. Spellman. An application of artificial neural networks to the prediction of surface ozone concentrations in the United Kingdom. *Appl. Geogr.* **19**:123–136 (1999).
13. G. Tkacz. Neural network forecasting of Canadian GDP growth. *Int. J. Forecasting* **17**:57–69 (2001).
14. J. Ellenius and T. Groth. Transferability of neural network-based decision support algorithms for early assessment of chest-pain patients. *Int. J. Med. Inform.* **60**:1–20 (2000).
15. J. Gasteiger, X. Li, and A. Uschold. The beauty of molecular surfaces as revealed by self-organizing neural networks. *J. Mol. Graphics* **12**:90–97 (1994).
16. J. Devillers. *Neural networks in QSAR and drug design*. Academic Press, London, 1996.
17. K. Takayama, A. Morva, M. Fujikawa, Y. Hattori, Y. Obata, and T. Nagai. Formula optimization of theophylline controlled-release tablet based on artificial neural networks. *J. Control Rel.* **68**:175–186 (2000).
18. K. M. Tolle, H. Chen, and H. Chow. Estimating drug/plasma concentration levels by applying neural networks to pharmacokinetic data sets. *Decis. Support Syst.* **30**:139–151 (2000).
19. K. K. Peh, C. P. Lim, S. S. Quek, and K. H. Khoh. Use of artificial neural networks to predict drug dissolution profiles and evaluation of network performance using similarity factor. *Pharm. Res.* **17**:1384–1388 (2000).
20. D. E. Rumelhart, G. E. Hinton, and R. J. Williams. Learning internal representations by error propagation. In D. E. Rumelhart and J. L. McClelland (eds.), *Parallel Distributed Processing: Explorations in the Microstructures of Cognition*, MIT Press, Cambridge, pp. 318–362.
21. R. M. Burton and G. J. Mpitsos. Event-dependent control of noise enhances learning in neural networks. *Neural Networks* **5**: 627–637 (1992).
22. C. P. Yu. C. K. Diu, and T. T. Soong. Statistical analysis of aerosol deposition in nose and mouth. *Am. Ind. Hyg. Assoc. J.* **42**: 726–733 (1981).
23. T. B. Martonen, I. Katz, K. Fults, and A. J. Hickey. Use of aerosol respirable fraction to predict lung deposition. *Pharm. Res.* **9**: 1634–1639 (1992).
24. C. F. Schiller, J. Gebhart, J. Heyder, G. Rudolf, and W. Stahlhofen. Deposition of monodisperse insoluble aerosol particles in the 0.005 to 0.2 μm size range within the human respiratory tract. Proceedings of the 6th symposium on inhaled particles. *Ann. Occup. Hyg.* **32**:41–49 (1989).
25. C. S. Kim. Methods of calculating lung delivery and deposition of aerosol particles. *Respiratory Care* **45**:695–711 (2000).